

Grid Monitoring and Protection with Continuous Point-on-Wave Measurements and Generative AI

Lang Tong^{1*}, Xinyi Wang¹ and Qing Zhao¹

^{1*}School of Electrical and Computer Engineering, Cornell University
Ithaca, 14850, NY, USA.

*Corresponding author(s). E-mail(s): lt35@cornell.edu;
Contributing authors: xw555@cornell.edu; [qz16@cornell.edu](mailto;qz16@cornell.edu);

Abstract

Purpose: This article presents a case for a next-generation grid monitoring and control system, leveraging recent advances in generative artificial intelligence (AI), machine learning, and statistical inference. Advancing beyond earlier generations of wide-area monitoring systems built upon supervisory control and data acquisition (SCADA) and synchrophasor technologies, we argue for a monitoring and control framework based on the streaming of continuous point-on-wave (CPOW) measurements with AI-powered data compression and fault detection.

Methods and Results: The architecture of the proposed design originates from the Wiener-Kallianpur innovation representation of a random process that transforms causally a stationary random process into an innovation sequence with independent and identically distributed random variables. This work presents a generative AI approach that (i) learns an innovation autoencoder that extracts innovation sequence from CPOW time series, (ii) compresses the CPOW streaming data with innovation autoencoder and subband coding, and (iii) detects unknown faults and novel trends via nonparametric sequential hypothesis testing.

Conclusion: This work argues that conventional monitoring using SCADA and phasor measurement unit (PMU) technologies is ill-suited for a future grid with deep penetration of inverter-based renewable generations and distributed energy resources. A monitoring system based on CPOW data streaming and AI data analytics should be the basic building blocks for situational awareness of a highly dynamic future grid.

Keywords: Grid monitoring, Generative AI, Continuous-point-on-wave measurements, Synchro-waveform, Power signal compression, Fault detection, and Overcurrent Protection.

1 Introduction

Over the past decades, the power grid has undergone unprecedented changes, from one with high-inertial synchronous generators dispatched to follow predictable demands to one with substantial non-dispatchable stochastic renewable resources integrated into the grid via power electronics operating at the nano-second time scale. With highly variable inverter-based resources (IBRs) such as wind/solar and reduced system inertia, the grid is increasingly stochastic and dynamic, frequently operating near its limits. Externally, accelerated occurrences of climate-related events put enormous stress on the aging grid. Outage events increased by 78% in the decade of 2011-2021 over the previous one [1], causing an average annual economic loss of over 150 billion dollars [2].

Not all outages can be prevented, but it begs the question: How many outages can be mitigated, load sheds restored quickly, and economic impacts minimized with today's technology and advances in computing, networking, and artificial intelligence?

This paper makes a case for a next-generation AI-powered grid monitoring system based on continuous point-on-wave (CPOW) measurements, providing high-resolution and high-fidelity grid monitoring and protection beyond the capability of the state-of-the-art synchrophasor technology. To this end, we present an AI-enabled data-streaming compression architecture and data-driven monitoring algorithms to detect anomalies and novel trends. Our approach is inspired by the classic Wiener-Kallianpur innovation representation of random processes [3, 4] and recent advances in generative AI capable of producing artificial random samples matching the originals.

1.1 Beyond PMU with CPOW Measurements

At the outset, it is highly relevant to address a cogent question: why should one consider new types of measurements when the phasor measurement units (PMUs) and synchrophasor technology can already provide synchronized measurements with resolutions higher than the state-of-the-art SCADA measurements? What can CPOW measurements reveal that SCADA and PMU measurements cannot?

PMU was invented over thirty years ago as a technology for wide-area situational awareness. The number of PMUs deployed in utilities in the US finally surpassed 3000 in 2022, far from adequate to cover the operation footprint of a small to medium-sized system operator. After three decades of (mostly governmental) investments worldwide and decades of extensive research, the technology has yet to take off. The unfulfilled promise of PMU is not because its technology is ahead of its time; PMU is based on the digital signal processing and the global positioning technologies of the seventies and eighties; both are inexpensive and widely used in commercial sensing and communication devices, including miniature wearable devices such as smartwatches and earbuds. It is difficult to foresee that PMU technologies can make significant impacts on reducing and preventing future blackouts.

One technical reason for the lack of deployment is that the 10 to 250 Hz reporting rates of the state-of-the-art PMU cover only a small fraction of significant grid events, as shown in Fig. 1. In particular, PMU extracts current and voltage phasors associated with the fundamental frequency of 50 or 60 Hz, removing the frequency contents

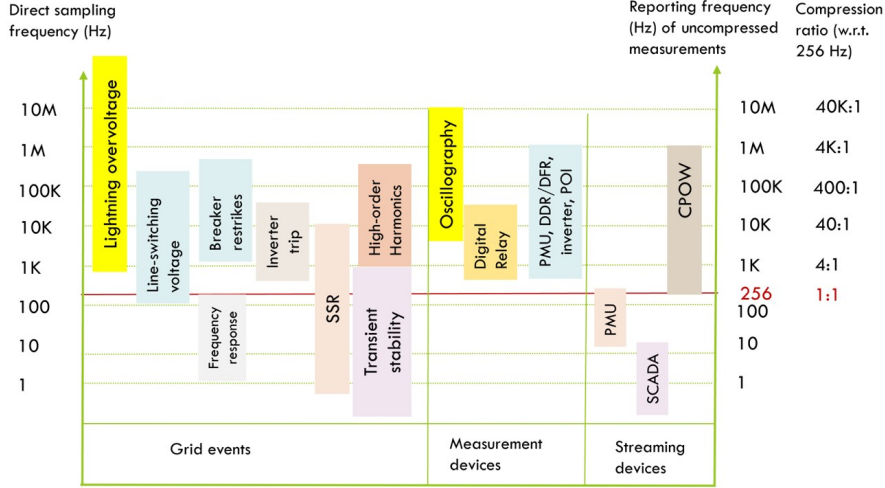


Fig. 1: Frequency contents of various grid events, each represented by a bar covering the range of the necessary Nyquist sampling rates on the left axis. The right axis shows the necessary reporting frequency of uncompressed measurement and the required compression ratio (relative to the 256 Hz PMU reporting rate.) This Figure is adapted from [5–8].

outside a narrow frequency band around the fundamental frequency. As such, PMU measurements are insensitive to most grid event waveforms shown in Fig. 1, unable to capture critical grid events when the network is under stress while producing too much data when the grid is normal. There is also the economic reason for the chicken-and-egg trap: insufficient monitoring resolution and coverage make PMU ineffective as a practical wide-area monitoring of impactful events, and the lack of compelling use cases limits necessary investments and broad deployments to realize its potential.

Interestingly, CPOW data are ubiquitous in modern grids in the form of direct Nyquist-sampled current and voltage waves. Measurements at all digital sensors, intelligent electronic devices (IEDs), PMUs, digital relays, and digital fault recorders are all CPOW data with sufficiently high sampling rates to capture highly dynamic signal waveforms from grid events. These high-resolution data rarely go beyond substations for grid situational awareness. Why not use CPOW data for high-resolution monitoring and control then? The common wisdom has been that (i) streaming CPOW measurements requires substantial infrastructure investments and bandwidth allocation; (ii) when the grid is in normal operating conditions, even PMU measurements are not “useful” most of the time. Why go with a technology with 10 to 100 times higher data rates?

The inadequate bandwidth argument against high-resolution CPOW streaming is unconvincing with today’s technology. Since the invention of PMU, the rate of communications has increased by nearly six orders of magnitude, and the world of communications has grown from zero cell phones to 5G/6G digital cellular, from text-based communications to real-time streaming of live sports events. Underlying all these

are signal processing and networking technologies that deliver high-fidelity entertainment and real-time control of robots, autonomous vehicles, and drones. If there are data communications technology barriers, they are by no means insurmountable.

The economic argument deserves more careful deliberation. Indeed, it seems wasteful to allocate bandwidth for contingencies that occur on rare occasions. It is also true that efficient data analytic methods are needed to sieve through large amounts of data in searching for early signs of network instability and actionable information. However, not having high-resolution data essential for a broad spectrum of grid events inhibits advances that can lead to breakthrough technologies critical to grid reliability and resiliency.

While not deployed in practice, the idea of using CPOW data for grid monitoring has been considered in the literature in recent years [6, 9–12]. Recent reviews of synchronized CPOW technology (a.k.a synchro-wave) are [13, 14], where the authors articulate broad visions of using CPOW data for monitoring, protection, and control. The work presented here aligns with these visions. We provide a possible architectural design and address data analytic challenges when measurements are highly stochastic.

1.2 Scope, Contributions, and Organization

This paper addresses two challenges in future grid monitoring systems: (i) efficient compression and communications for real-time streaming of CPOW measurements within the current bandwidth limits for PMU streaming technology and (ii) rapid and reliable detection of faults and novel trends from highly stochastic CPOW measurements.

The main contribution of this work is twofold. First, we develop a novel compression architecture that combines machine-learning-based data analytics and data compression for CPOW data streaming. Such technology is critical for bandwidth-efficient, dynamic, and interactive operations among IEDs, substations, and the control center during severe grid events. Second, we propose a sequential detection approach for the reliable and rapid detection of anomalies and novel trends from CPOW data streaming. Built on the classic innovation representation of time series pioneered by Wiener and Kallianpur, the proposed generative machine learning technique distinguishes the normal and the faulty in the feature domain of the underlying probability distributions of CPOW data, in contrast to conventional methods that directly compare current and voltage phasors with their nominal values. Finally, we apply the proposed anomaly detection approach to over-current protection in distribution systems, where the presence of distributed stochastic generations causes protection blinding and sympathetic tripping. We demonstrate 16% improvements in detection accuracy and 67.9% in detection speed.

This paper is organized as follows. Section 2 describes a generative AI approach to representation learning of high-resolution time series (such as that from CPOW data streaming), which transforms the generic nonparametric time series to a canonical independent and identically distributed (IID) innovation sequence by an *innovation autoencoder*. This particular autoencoder structure plays a key role in both CPOW data compression and anomaly detection. In particular, anomaly detection problems are formulated and solved as nonparametric hypothesis testing with arbitrary and

unknown distributions. Section 2.3 presents a machine-learning (ML) based data compression aimed at achieving the optimal compression rate-distortion tradeoff. Section 3 presents the application of the proposed anomaly detection in over-current protection.

Notations used in this work are standard. Random variables are nominally denoted by capital letters, and their realizations in small letters. Vectors, matrices, and sequences are usually in boldface. We use $\mathbf{X} = (X_t)$ to represent a random sequence and $\mathbf{x} = (x_t)$ its realization. When considering a segment of a random sequence, $\mathbf{X}_{t_1:t_2}$ denotes the segment from t_1 to t_2 , *i.e.*, $\mathbf{X}_{t_1:t_2} = (X_{t_1}, \dots, X_{t_2})$. For two random variables X and Y , $X \stackrel{\text{a.s.}}{=} Y$ means the two equal almost surely and $X \stackrel{\text{d}}{=} Y$ equal in distribution. Table 1 gives a list of designated symbols.

Table 1: Mathematical notations used in this paper.

(X_t)	The random process representing a sequence of CPOW measurements.
(V_t)	The innovation sequence.
(U_t)	An IID sequence of uniform distribution.
(\hat{X}_t)	The reconstructed sequence output by IAE decoder.
(x_t)	A sequence of real numbers indicating the past observations of (\mathbf{X}_t) .
G	Innovation encoder function.
H	Innovation decoder function.
G_θ	A neural network approximation of G parameterized by θ .
H_η	A neural network approximation of H parameterized by η .
D_γ	Innovation discriminator that measures the distance between (\mathbf{V}_t) and (\mathbf{U}_t) .
$\mathcal{U}[0, 1]$	The continuous univariate uniform distribution on $[0, 1]$.

2 Learning Innovation Representations

The proposed AI-powered monitoring and anomaly/novelty detection approaches are rooted in the classic idea of innovation representation of time series first proposed by Wiener and Kallianpur [3], who made a profound conjecture that stationary random processes can be represented by an IID uniform (or Gaussian) *innovation sequence*. By removing temporal dependencies and converting a generic stationary process to a canonical IID sequence with simple uniform/Gaussian marginals, the innovation representation is arguably the most efficient representation of a nonparametric random process.

2.1 Wiener-Kallianpur Innovation Representation

In the parlance of modern machine learning, an innovation representation of a stationary random process (X_t) is a *causal autoencoder* shown in Fig. 2, with the latent process (V_t) being an IID-uniform *innovation sequence*. As suggested by the word *innovation*, V_t represents the new information contained in X_t not present in (*i.e.*, statistically independent of) the past $\mathbf{X}_{0:t} = \{X_{t-1}, X_{t-2}, \dots\}$.

Mathematically, the innovation representation of the time series is defined by a pair of causal mappings (G, H) and the innovation sequence (V_t) :

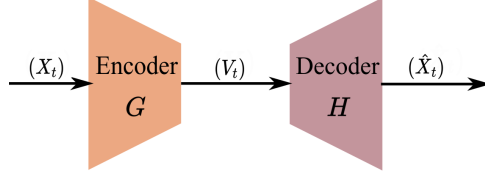


Fig. 2: An autoencoder interpretation of innovation representations.

$$V_t = G(X_t, X_{t-1}, \dots), \quad (V_t) \stackrel{\text{iid}}{\sim} \mathcal{U}[0, 1], \quad (1.1)$$

$$\hat{X}_t = H(V_t, V_{t-1}, \dots), \quad (\hat{X}_t) \stackrel{\text{a.s.}}{=} (X_t). \quad (1.2)$$

By matching (almost surely) the autoencoder output (\hat{X}_t) with its input (X_t) , Wiener-Kallianpur’s innovation representation is an ideal architecture for the compression and reliable communications of nonparametric random processes in the (Shannon) information-theoretic sense.

The idea of innovation representation became popular in engineering in the 1960s [15], especially in signal processing and control. The measurement-update step in Kalman filtering is an example of how innovations are used in estimation, prediction, and control. Despite the generality of the Wiener-Kallianpur innovation representation, its practical applications are limited to Gaussian and additive Gaussian models—the only two cases when causal autoencoder (G, H) can be constructed explicitly and implemented in practice. No general computationally tractable way to extract the innovations sequence exists, even when the underlying probability distributions of (X_t) are known. Outside the recent work of [16], no existing work is capable of learning the innovation representation.

2.2 Learning Innovation Representation

In [16], the authors proposed a generative adversary network (GAN) based approach to learning the Wiener-Kallianpur innovation representation by jointly minimizing the Wasserstein distance between the latent process and the uniform IID process and the mean-squared error (l_2 distance) of the autoencoder output as an estimate of the input. The structure of the deep learning approach to innovation representation is shown in Fig. 3.

The encoder G_θ and decoder H_η are *causal* convolutional neural networks parameterized by coefficients θ and η , respectively. These parameters are optimized to match the autoencoder output \hat{X}_t with its input X_t (in the mean-squared sense) and impose constraints that the latent process (V_t) is an IID process. Here, we consider two possible types of innovations: the IID-uniform innovations as in [16] suitable for anomaly detection and IID-Gaussian for compression and communications. The latter is a slight but new variation designed to match the compression with the typical additive Gaussian characteristics of communication channels.

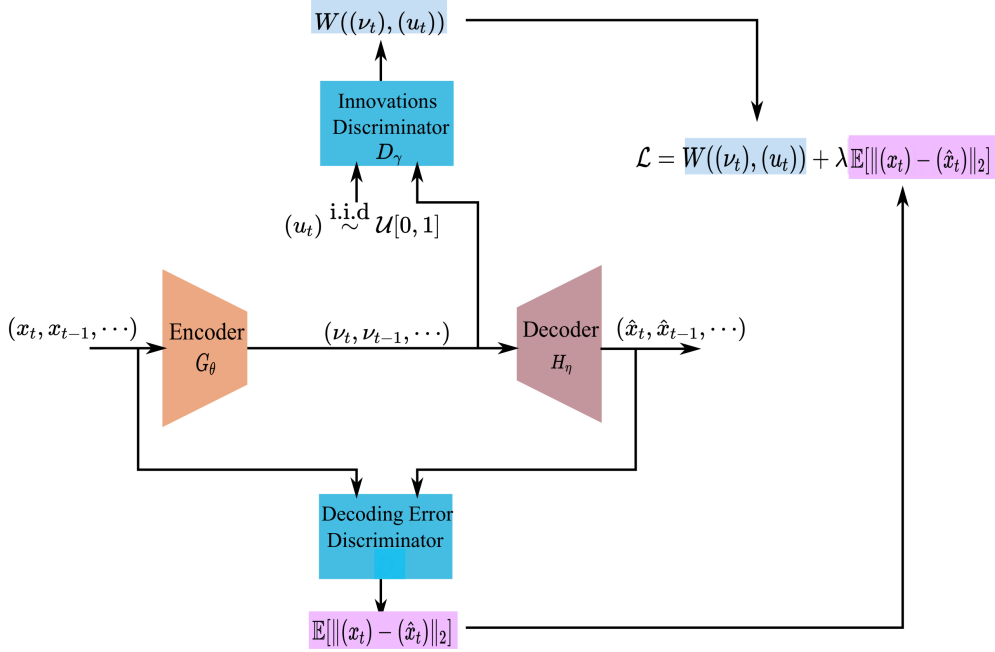


Fig. 3: A Machine Learning Architecture for Innovation Representation.

The learning algorithm of the autoencoder (G_θ, H_η) and discriminator D_γ is of the GAN type with parameters (θ, γ, η) jointly optimized from the l_2 -Wasserstein distance measures:

$$L((X_t), \theta, \eta) := \max_{\gamma} \left(\mathbb{E} \left[D_\gamma((V_t), (U_t)) \right] + \lambda \mathbb{E} \left[\|(\hat{X}_t) - (X_t) \|_2 \right] \right) \quad (2)$$

$$(\theta^*, \eta^*) := \arg \min_{\theta, \eta} L((X_t), \theta, \eta), \quad (3)$$

where U_t is the IID-uniform random sequence and λ a real number to bring two distance measures to the same scale. Since the two parts of loss function (2) regularize (G_θ, H_η) according to (1.1) & (1.2), minimizing the loss with respect to θ and η is thus equivalent to enforcing (V_t) being IID uniform/Gaussian, and (\hat{X}_t) being close to (X_t) .

In practice, finite-dimensional neural network input and finite-dimensional segments of random processes are used. In [16], structural convergence is established to show that the finite-dimensional implementation of the autoencoder converges to the theoretical infinite-dimensional innovation representation, as the dimensionality of the deep-learning architecture grows.

2.3 Anomaly and Novelty Detection

We present an innovation-based approach to anomaly and novelty detection, where the underlying probability models are unknown under normal and abnormal conditions. In

particular, we consider a prototype hypothesis testing model involving random CPOW measurement $\mathbf{X} = (X_t)$ either at a local IED, a substation, or at a control center:

$$\mathcal{H}_0 : \mathbf{X} \sim P_0 \text{ vs. } \mathcal{H}_1 : \mathbf{X} \sim Q \in \mathcal{Q}. \quad (4)$$

The null hypothesis \mathcal{H}_0 represents data under normal operating conditions when CPOW measurement \mathbf{X} is a random process following unknown probability distribution P_0 . We assume that training data are available to learn an innovation representation of \mathbf{X} discussed in Sec. 2 via offline or online learning. It is reasonable to assume that historical data under \mathcal{H}_0 are plentiful.

The alternative hypothesis \mathcal{H}_1 models the scenario when anomalous CPOW measurements follow an unknown distribution $Q \in \mathcal{Q}$. We do not specify the anomaly types, as they may not be enumerable. Nor do we assume that there are historical data to learn \mathcal{Q} because, in practice, validated historical data for anomalies are rare.

The anomaly detection model (4) can be generalized for detecting new phenomena that are not necessarily faulty. Such a novelty detection problem can be modeled by

$$\mathcal{H}_0 : \mathbf{x} \sim P \in \mathcal{P} \text{ vs. } \mathcal{H}_1 : \mathbf{x} \sim Q \in \mathcal{Q}. \quad (5)$$

where $\mathcal{P} = \{P_0, \dots, P_K\}$ is a dictionary of observation classes identified and validated in the past, making hypothesis \mathcal{H}_0 composite. With autoencoders associated with each $P_i \in \mathcal{P}$ learned, the detection approach developed here can be applied.

Related Work

The detection model (4) belongs to the category of nonparametric hypothesis testing [17], for which classical approaches in statistics generally assume known probability model P under \mathcal{H}_0 . Standard techniques such as the Kolmogorov-Smirnov test and others [18] can be used for offline detection involving non-sequential data with a known model under \mathcal{H}_0 .

Modern machine learning removes the assumption of known probability models under both \mathcal{H}_0 and \mathcal{H}_1 , though techniques specializing in anomaly/novelty detection in time series are limited because the probability structures for nonparametric time series are infinite-dimensional. Standard approaches reduce the problem to a finite-dimensional approximation by considering finite-duration segments of time series samples. See, *e.g.*, [19–21]. Such segmentations overlook the temporal dependencies of the time series, which are crucial in anomaly/novelty detection unless the segments are chosen to be very large. This results in a long detection delay and intractable computation complexity.

With an unknown probability model under \mathcal{H}_0 , the state-of-the-art approaches roughly fall into three categories. One is based on classifiers such as the one-class support vector machine [22] and its many variants for different applications [23–25]. Such techniques *implicitly* assume that the support of the anomalous CPOW data distribution is largely disjoint from that of the anomaly-free. With only training data under \mathcal{H}_0 , these techniques perform poorly when anomaly and anomaly-free models have overlapping support domains.

The second group of techniques simulates samples under \mathcal{H}_1 using hypothetical distributions some distance away from that under \mathcal{H}_0 [26–28]. It is, however, difficult to capture all possible alternative distributions. The third category captures many machine learning solutions developed in recent years, where the detection is performed in a transformed “feature domain”, where some types of confidence scores on the learned anomaly-free model are used to detect anomaly [29–32]. As shown in [33], however, even with the perfect density estimate, detection may still perform poorly. Most relevant to our approach are the autoencoder-based machine-learning techniques for anomaly/novelty detection problems. See *e.g.*, [24, 25, 34–36]. The use of independent component analysis in [35, 36] bears a structural resemblance to the innovation approach, with the main difference lying in the requirement of causality on the autoencoder and training in our approach. Graphical models have been proposed to exploit graphical structures exhibited in the training data under \mathcal{H}_0 [37–39]. Such techniques need to be better explored, especially in the context of detecting anomalies in time series.

With the phenomenal success of natural language processing, the idea of “transformer” has gained a large following, and there have been successful demonstrations recently in classification and some time series forecasting problems [40, 41]. The applicability of these techniques in power systems remains to be determined as power system data do not have the long-range dependencies typical natural language models, making the high-dimensional transformer-type of language models difficult to learn [42].

Detection via Innovation Representation

The approach presented here is based on the innovation representation discussed in Sec. 2 and was originally developed in [16, 43]. The most striking feature of the innovation-based anomaly detection is that the innovation autoencoder transforms the problem of anomaly detection with an unknown probability model under \mathcal{H}_0 to one under the known and simple model of IID uniform (or Gaussian). The new contribution here is the application of Neyman’s Smooth Test (NST) for anomaly detection and a sequential technique for quick detection.

Let (V_t) be the innovation sequence of the Wiener-Kaillanpur autoencoder (G, H) . The anomaly detection model (4) is transformed to the feature space of innovations

$$\mathcal{H}_0 : (V_t) \stackrel{\text{IID}}{\sim} \mathcal{U}([0, 1]) \text{ vs. } \mathcal{H}_1 : (V_t) \text{ is not IID-uniform.} \quad (6)$$

While the underlying hypothesis testing problem remains challenging because of the arbitrariness and the uncountable nature of the alternative probability models under \mathcal{H}_1 , the innovation representation provides a bridge to the classical Goodness-of-Fit (GoF) problem, for which considerable literature exists [44].

Neyman proposed the NST in 1937 [45] for testing (6) when the probability distribution under \mathcal{H}_1 is “smooth.” In the contemporary machine learning language, NST employs the orthogonal Legendre polynomial kernels $\{\pi_k\}$ as a kernel representation of probability distributions under \mathcal{H}_1 . The schematic of NST is shown in Fig. 4 where inputs (v_t) are passed through Legendre polynomial kernels at the input layer. The

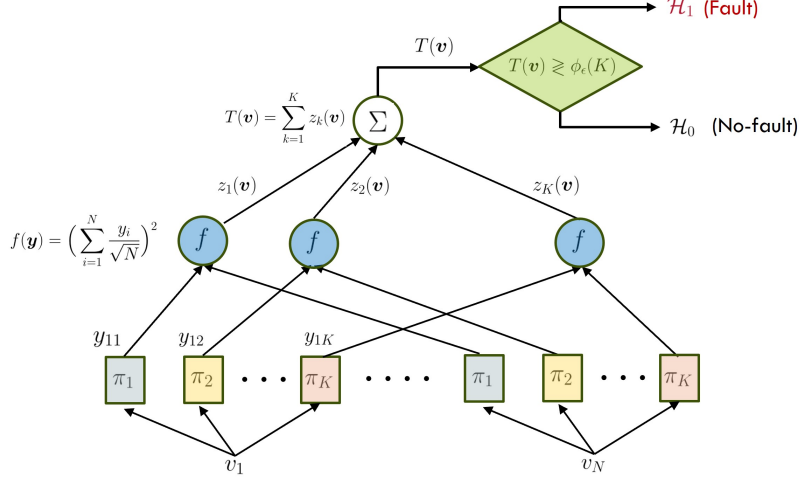


Fig. 4: Neyman's Smooth Test (NST).

output of the input layer is the sum of independent random variables at the Central-Limit Theorem scaling, resulting in a limiting Gaussian distributed $\sum_i y_i / \sqrt{N}$, and χ^2 distributed $T(\mathbf{v})$ with K -degree of freedom, asymptotically. The testing is a threshold decision based on

$$\sum_{i=1}^K \left(N^{-1/2} \sum_{t=1}^N \pi_i(v_t) \right)^2 := T(\mathbf{v}) \underset{\mathcal{H}_0}{\overset{\mathcal{H}_1}{\gtrless}} \phi_\varepsilon(K), \quad (7)$$

where $\phi_\varepsilon(K)$ is the $(1 - \varepsilon)$ -quantile of a Chi-square distribution with K degrees of freedom. Parameter ε can be chosen according to the desired false positive rate.

NST was shown to be the locally most powerful test for uniformity testing [45], outperforming all other possible detection techniques in a neighborhood around the null hypothesis \mathcal{H}_0 . In Rayner and Best [46], the author declared: “don’t use those [other] methods—use a smooth test!”

3 Compression and Data Analytic Architecture

This section presents an innovation-based compression and data analytic architecture that combines subband coding, innovation representation, and local/central anomaly/novelty detection. The schematic of the proposed compression system is shown in Fig. 5 with key components explained next.

The upper branch of Fig. 5 is the schematic for an IED that takes analog current/voltage measurement $x(t)$. Power system signals are narrow passband signals with special subband spectral structure illustrated in Fig. 5. Around the fundamental frequency $\pm f_0$ is the fundamental frequency band regulated with frequency deviations within W_0 . Typically $W_0 < 1$ Hz. Above the fundamental frequency band are harmonic

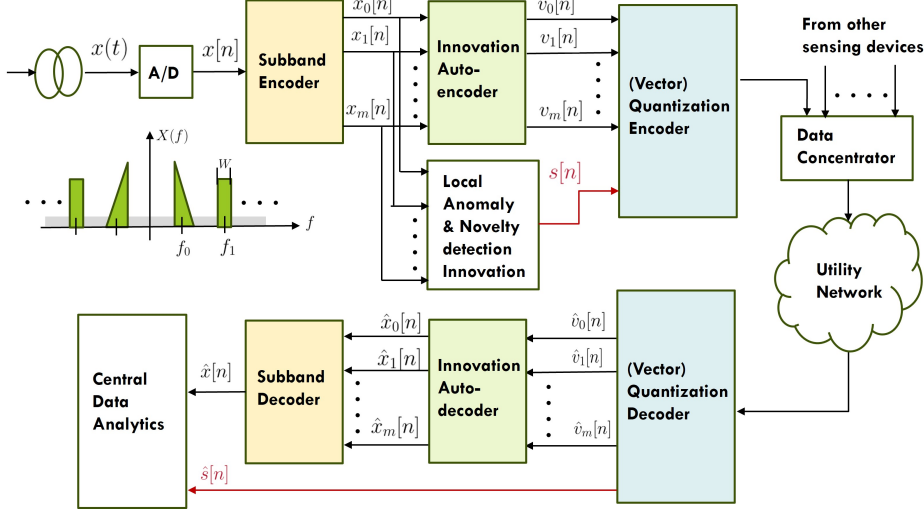


Fig. 5: A schematic of the innovation-based compression.

subbands at the multiples of f_0 , $f_k = kf_0$, that account for higher-order harmonics due to nonlinear devices in the network. There may also be inter-harmonic frequency components represented by the grey area. Higher-order harmonics and inter-harmonics may appear sporadically; they are modeled as on-off random processes.

Subband Coding

The A/D converter samples $x(t)$ at the Nyquist rate to obtain a digital CPOW signal $x[n]$. Depending on the spectral bandwidth of $x(t)$, the Nyquist sampling rate is typically in the tens of kHz (or higher) range, resulting in more than 600 K samples per cycle. The subband coding scheme proposed in [5] greatly reduces the Nyquist-sampled data rate via the subband decomposition and encodes each harmonic (and inter-harmonic) subband separately. By the passband Nyquist sampling theorem, a harmonic subband with passband bandwidth W requires only a $2W$ sampling rate. For instance, if the fundamental subband has the bandwidth of $W_0 = 1$ (Hz), one sample per 30 cycles is sufficient to capture the signal in the fundamental frequency band fully. For an m harmonic-subband spectrum, each with W Hz passband bandwidth, $mW/30$ samples per cycle are sufficient for lossless compression. The subband coding block extracts the baseband components of $X(f)$, down-sampling the Nyquist-sampled data to achieve two to three orders of magnitude data rate reduction. The subband coding technique is well developed for multi-media compression and is embedded in practical audio/video communications data-streaming technologies. The subband encoder proposed in [5] can be easily implemented by off-the-shelf filter banks. See details in [5]. Note the per-cycle data samples of the subband CPOW signals $\{(x_i[n])\}$ are baseband representations of the signal spectrum, typically at the rate of less than one sample per cycle under normal operating conditions.

Innovation Autoencoder and Local Data Analytics

While the subband coding scheme significantly reduces the data rate of the direct Nyquist sampled $(x[n])$, further data rate reductions can be achieved through information-theoretic approaches that offer an optimal tradeoff between the compression rate and distortions of reconstruction. Additional data rate reduction can be achieved through local data analytics that adaptively selects harmonic subbands for transmission. For instance, harmonic and inter-harmonic subbands may be inactive under normal operating conditions. During significant network events, signal contents from only a few harmonic subbands may be informative.

The innovation autoencoder discussed in Sec. 2 is used to transform subband signals $\{(x_i[n])\}$ to a set of innovations sequences $\{(v_i[n])\}$, each is an IID uniform or Gaussian sequences. For minimum data compression over the typical additive Gaussian noise channel of the utility network, it is natural that the innovation sequence $(v_i[n])$ is IID Gaussian with matching mean and variance with $(x_i[n])$, from which optimal bits-allocation to each subband innovations can be determined. This is discussed as part of the vector quantization encoder in Sec. 3.

The local data analytics unit detects anomalies and novelties using techniques presented in Sec. 2.3. The local data analytics unit produces the local state sequence (s_t) that can be used to compress data further and provide summary statistics for the control center. Specifically, (s_t) may include the normal/fault state sequence and estimated fault locations when faults are detected locally. Under the normal system state, data from many subbands can be suppressed, and the control center can recall the suppressed signal if necessary.

Vector Quantization Encoder

Vector quantization converts innovations and state sequence $\{(v_i[n]), s[n])\}$ to bit-streams to be transmitted over the utility network (after multiplexing with bit streams from other IEDs.) The quantization schemes developed in [5] can be used. The new feature considered here is an information theoretic approach to compression not included in [5].

Consider the IID-Gaussian innovation sequences $(V_i[n])$, with mean and variance (μ_i, σ_i^2) for the i th subband innovations. Given the acceptable mean-square distortion of the reconstruction $D_i := \mathbb{E}(\hat{X}_i[n] - X_i[n])^2$, the optimal compression is achieved by allocating distortion D_i to subband i constrained by $D = \sum_i D_i$ through the so-called inverse water-filling procedure [47]. The Gaussian rate-distortion function gives the minimum transmission rate subject to distortion measure

$$R(D) = \sum_{i=1}^m \frac{1}{2} \log \frac{\sigma_i^2}{D_i}.$$

There are many practical vector quantization schemes [48], including some of the machine learning techniques.

Decoder at Substations or Control Center

The lower branch of Fig. 5 describes the building blocks of the decoding process at the control center. For the most part, this process is the inverse of the upper branch, following mostly the procedure described in [5]. The vector quantization decoder reproduces the innovation sequence $\{(\hat{v}_i[n])\}$ for each subband (for those subbands that are not suppressed.) The innovation autodecoder is used to produce the decompressed subband signal $\{(\hat{X}_i[n])\}$ (in the baseband form), and the subband decoder assembles the subband signal to form $\hat{x}[n]$ as the estimation of the original CPOW $x[n]$, for which the estimation error is controlled by D in the rate-distortion function.

Central Data Analytics and Interactive Networking

Integrating data analytics with compression and networking provides the key component for interactive networking: the local IEDs can initiate the interaction based on local detection and transmit anomalous waveforms. Likewise, with the received data feeds from multiple IEDs, the central data analytics unit can initiate requests for high-resolution data when data feeds result in ambiguities and inference with low confidence. Here, we do not discuss networking protocols that realize such interactive networking.

4 Over-current Fault Detection and Protection

Traditional power system protection is based on a deterministic power system model. For short circuit faults, a pre-determined threshold (the pickup current) is set such that current flows exceeding the threshold trigger relay actions. The significant presence of distributed stochastic generations and IBRs causes two types of erroneous relay actions. One is the so-called *protection blinding* shown on the left panel of Fig. 6, where the stochastic distributed generation (SDG) offsets the high current flow through the protection device (PD), causing Type II (miss-detection) error in PD's decision. The second type is the *sympathetic tripping* shown on the right panel of Fig. 6, where the PD experiences high current flow from SDG, causing a Type I (false alarm) error and a PD's unnecessary tripping action.

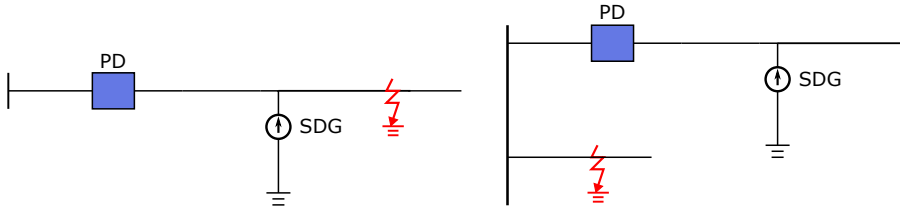


Fig. 6: Two types of erroneous protection actions caused by stochastic distributed generation. Left: Protection blinding. Right: Sympathetic tripping.

Related Work

Power system protection under stochastic and distributed generations is an active area of research because of the increasing integration of power electronics-based resources. In [49], a detailed characterization and classification of distribution system protection under bulk renewable energy sources is provided. Classical techniques are “hard-wired” that directly compare the measurements with fixed threshold [50]. Other methods include installing fault current limiter [51, 52] to mitigate the effect of SDG or view pickup current as the decision variables to an optimization program, taking into account network configurations [53, 54].

More sophisticated data-driven solutions have been proposed. Methods belonging to this category design pickup current settings corresponding to different DG output levels, and the DG conditions are usually classified via data-driven methods [55]. In [56], fuzzy logic is applied to determine the DG working states and transferred to relays to adjust their setting. The authors of [57] applied wavelet transformation to measurements and adopted a neural network to detect the Ferroresonance for the wind farm system. Relay settings can also be computed from estimated system parameters of a Thevenin equivalent system [58] or based on steady-state fault current [59]. Other data-driven methods are developed for networked sensors as a multi-agent system [60], assuming a network supporting communications among agents. The method proposed in [61] adjusts the over-current relay setting based on current measurements from relays downstream.

4.1 Innovation-Based Sequential Fault Detection

We propose an innovation-based sequential fault detection (ISFD) approach to reduce protection errors and decision time. ISFD is a data-driven approach that makes testing decisions based on the latent process of the innovation autoencoder trained with anomaly-free realizations of possibly multiple stochastic CPOW measurements. In contrast, conventional techniques typically compare current phasor magnitudes with a pre-determined threshold. Such approaches are vulnerable to stochastic distributed generations, resulting in high false positive and negative rates that lead to sympathetic tripping and protection blinding, respectively. ISFD uses empirical distribution-related statistics to separate normal from faulty measurements when, in the time domain, the waveform corresponding to the two cases is very close. This is an instance in which choosing the right feature for detection is crucial.

ISFD is designed to achieve short detection delay by implementing a sequential version of NST based on the classical notion of change detection. When distribution statistic shows that the distribution of observed CPOW has a large distance from the normal distribution P_0 under \mathcal{H}_0 , the procedure terminates quickly by declaring fault. When the observed CPOW is close to P_0 under \mathcal{H}_0 , the observed data will likely be from a normal waveform. No alert is necessary, but more data are collected to enhance detection accuracy.

ISFD implements the above sequential procedure using the so-called doubling search technique [62]. At each iteration, ISFD executes NST with a fixed-sized batch of samples. If the output of the detecting technique is \mathcal{H}_0 , the batch size will be doubled, and the detecting technique will be re-run in the next iteration. An upper bound

on the number of iterations is often set to avoid infinite detection delay. The detailed algorithm of the doubling search trick implementation of NST is presented in Algorithm 1. Once NST has made its detection decision, its decision is passed to the circuit breaker to carry out its protection action.

Algorithm 1 A doubling search implementation of a K -th order Neyman’s smooth test at time t^* .

Input: innovations data (v_t) , order of Legendre polynomials K , minimum separation λ , target false positive rate ε , and a scaling constant C .
 Compute threshold $\phi_\varepsilon(K) := \inf\{\phi : \Pr[Q > \phi] \leq \varepsilon, Q \sim \chi^2(K)\}$
 Output = \mathcal{H}_0 .
for $i = 1, 2, \dots, \log_2 \lambda$ **do**
 $N = 2^i C$
 Draw N samples of $(v_{t^*}, v_{t^*+1}, \dots, v_{t^*+N-1})$
 if $N^{-1/2} \sum_{i=1}^K \sum_{t=t^*}^{t^*+N-1} \pi_i(v_t) > \phi_\varepsilon(K)$ **then**
 Output = \mathcal{H}_1
 Break
 end if
end for
 Report Output to the executor (circuit breaker).

4.2 Performance Evaluations

Simulation setting

We evaluated the performance of ISFD and two competing methods using the IEEE 13-bus distribution network shown in Fig. 7. To account for randomness in the measurements introduced by renewable energy resources, we added a 1MW DG controlled by real-world current profile collected at the micro-grid located in EPFL between node 692 and 675. The DG was driven by EPFL’s current profile at the battery connection¹, and current measurement samples were collected at 50KHz sampling frequency. The entire system is simulated through MATLAB/Simulink.

Fig. 7 shows multiple fault scenarios considered in the simulation study, with red arrows indicating fault locations and blue boxes for the protective relays. We simulated single-phase short circuit faults for each fault location, using MATLAB Simulink to generate CPOW measurements. Specifically, fault F1 and F3 were chosen to test the impact of SDG under sympathetic tripping whereas F2 was chosen to evaluate the system’s performance under protection blinding.

When a single-phase short circuit fault happens at F1, R3 is the primary relay for F1 and R2 a backup. During F1, sympathetic tripping at R4 may occur because the current feed from SDG downstream could increase significantly. Similarly, when F3 happens, R4 is also subject to sympathetic tripping due to current flow from downstream DG. In this case, the primary relay is R2 and the backup R1. On the other

¹Data can be found here: <https://github.com/DESL-EPFL/Point-on-wave-Data-of-EPFL-campus-Distribution-Network>

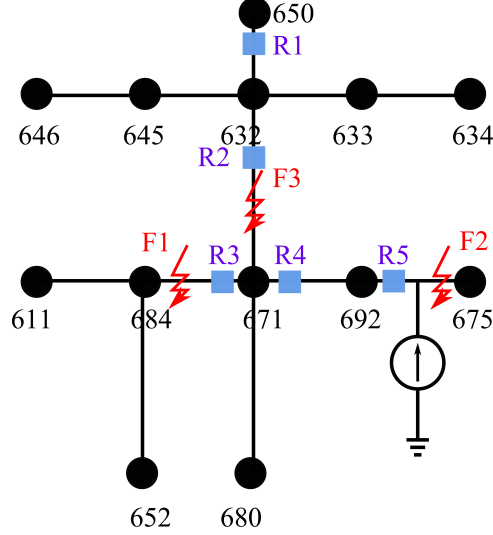


Fig. 7: IEEE 13 Bus System Configuration.

hand, the primary relay R5 for fault scenario F2 faces protection blinding because of DG's support for current and voltage at R5 during fault at F2.

Algorithm Implementations and Performance Metrics

We compared ISFD with two overcurrent protection baselines: (i) the “conventional” over-current relay protection with predetermined a fixed pickup current and inverse time function defined by the IEEE 37112 standard [63], and (ii) AOCR—an adaptive method proposed in [64]—with pickup current as a linear function of 10-second moving-average current and minimum fault current in the zone.

All three methods required detection threshold settings. The ISFD threshold can be obtained analytically for a given false positive rate (FPR). In contrast, the threshold settings for the conventional and AOCR methods were obtained empirically through simulations to meet the FPR target.

In the experiments, ISFD was implemented based on a 4th-order Neyman's smooth test with the doubling search procedure as described in Algorithm 1. We chose $C = 42.5$ and $\lambda = 20$. We generated 10,000 samples under the anomaly-free condition for innovation autoencoder training. We adopted Adam optimizer with $lr = 1e-5$ to train the innovation autoencoder. The threshold of the conventional method and AOCR are chosen manually to cap the FPR at 0.05. The inverse-time characteristics of these two over-current relay-based methods are chosen according to the moderately inverse characteristics in IEEE standard [63].

We evaluate the performance of each protection scheme by True Positive Rate (TPR), False Positive Rate (FPR), and detection delays. For each fault scenario, we conducted 1,000 independent runs of the same system, driving the SDG current profile with 1,000 different trajectories learned from the EPFL dataset. The trajectories were learned through a weaker version of innovation autoencoder (WIAE) with the l_2

distance between (X_t) and (\hat{X}_t) in the learning objective replaced by the Wasserstein distance. WIAE was trained by the EPFL current profile, and SDG current trajectories from the same distribution as the EPFL current profile can then be drawn as the output sequence (\hat{X}_t) of the decoder. The detailed implementation of WIAE can be found on Github². All metrics were calculated through 1,000 Monte Carlo runs.

Results

Table 2 shows the test results. For each method deployed at the locations of different relays, their TPR, FPR, and delays were computed from Monte Carlo runs conditioned on no-faults and faults F1, F2, and F3.

Table 2: Detection Results for Different Fault Scenarios of IEEE 13-bus System.

Location	Relays	Method	TPR	FPR	Delay(s)
F1	R3 (primary)	ISFD	1	0.0451	0.0017
		AOCR	0.9893	0.0309	0.0175
		Conv.	0.9940	0.0402	0.0102
	R2 (backup)	ISFD	0.9991	0.0255	0.0068
		AOCR	0.9894	0.0097	0.0236
		Conv.	0.9942	0.0500	0.0143
	R4 (sympathetic tripping)	ISFD	0.0779	0.0453	N/A
		AOCR	1.0	0.0052	0.0301
		Conv.	1.0	0.0093	0.0441
F2	R4 (backup)	ISFD	0.9982	0.0492	0.0136
		AOCR	0.4260	0.0414	0.0340
		Conv.	0.5569	0.0450	0.0133
	R5 (primary)	ISFD	0.9875	0.0371	0.0017
		AOCR	0.7118	0.0490	0.0221
		Conv.	0.6425	0.0415	0.0053
F3	R1 (backup)	ISFD	0.9927	0.0482	0.0068
		AOCR	0.8912	0.0409	0.0234
		Conv.	0.4447	0.0341	0.0211
	R2 (primary)	ISFD	0.9818	0.0385	0.0017
		AOCR	0.8847	0.0501	0.0233
		Conv.	0.4487	0.493	0.0187
	R4 (sympathetic tripping)	ISFD	0.0593	0.0257	N/A
		AOCR	0.9939	0.0025	0.0311
		Conv.	1	0.0043	0.0422

²<https://github.com/Lambelle/WIAE>

True Positive Rate of Detection: From the TPR column evaluated under faults F1, F2, and F3, respectively, the primary and backup relays should trip for all faults. We see that ISFD achieved the best detection accuracy for the primary and backup relays whenever a relay served as either a primary or a backup under all three faults. For example, under F1, the fault detection rate is 100% at the primary relay R3 and 99.91% at the backup relay R2. Similar performance were observed under F2 and F3. ISFD did have sympathetic tripping due to false positive detection at Relay R4 7.8% of the time due to the presence of SDG.

Both AOCD and the conventional did not perform well at the primary relay R3 under all three faults with detection rates under 90%. At the backup relays, AOCD and the conventional performed well under F1 but insufficient under F2 and F3. Sympathetic tripping occurred 100% of the time under F1 and F3.

False Positive Rate of Detection: All methods achieved FPR smaller than 5%, since we computed their corresponding decision threshold by setting their empirical FPRs to be 0.05, analytically or empirically. In particular, for ISFD, the decision threshold is computed analytically, and its FPR under all cases is smaller than 5%, showing that the innovation autoencoder transformer current measurements to IID uniform samples effectively.

Detection Delay: The delay column shows how quickly the detection decisions were rendered by the three methods. ISFD significantly outperformed both AOCD and the conventional, reducing the detection time by 90% at primary relays. At backup relays, ISFD performed better for most cases except under F1 (worse than AOCD) and under F2 (comparable with the conventional).

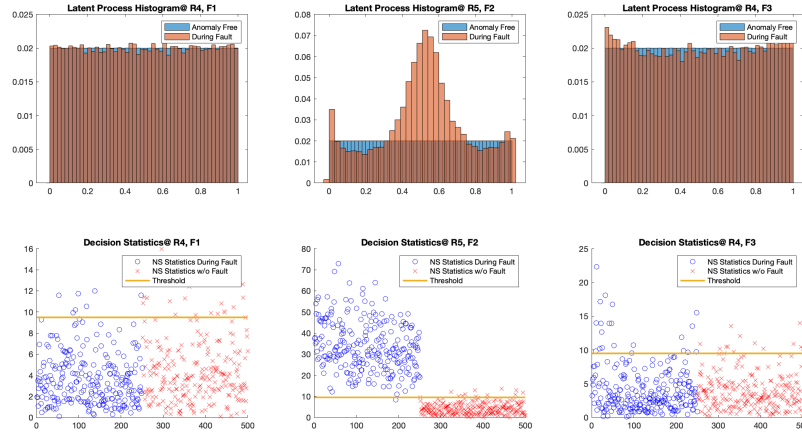


Fig. 8: Top row: Histogram of the latent sequence generated by the innovation autoencoder. Bottom row: the scatter plots of decision statistics.

Insights

To gain insights into the test results, we plotted the decision statistics of each method with 250 Monte Carlo runs each for both anomaly and anomaly-free cases, marked in circles and crosses, respectively.

Test statistics under ISFD: For ISFD, we plotted the histogram of the innovation sequence associated with the current CPOW measurements under three faults in Fig. 8. The top row of the figure shows the histograms of the latent processes under three faults. The bottom row shows the scatter plots of ISFD’s decision statistics.

The leftmost panel shows the case of F1 at R4 unrelated to F1. For this case, the test should be negative had there been no SDG. The top-left and top-right figures show that the histograms of the latent processes were approximately uniform, indicating that the observations were deemed normal. The scatter plots below show that the Neyman smooth test statistics were below the threshold most of the time. Thus the rates of positive tests was about 7% and 5%, respectively.

The middle panel shows the case of F2 at R5. As the primary relay, R5 should trip with low detection delays. The top-middle figure shows that the distributions of innovations under fault and no-fault cases exhibit clear distinctions. The anomaly-free histogram was uniform, whereas the anomalous one showed significant deviation from the uniform distribution. Consequently, Neyman smooth test statistics for the anomalous case were mostly above the decision threshold, resulting in a TPR higher than 98%.

Test statistics under the conventional method: For the conventional method, the test statistic was based on the pickup current. We plotted the maximum current magnitude in each decision block with decision threshold I_{pickup} , shown in Fig. 9.

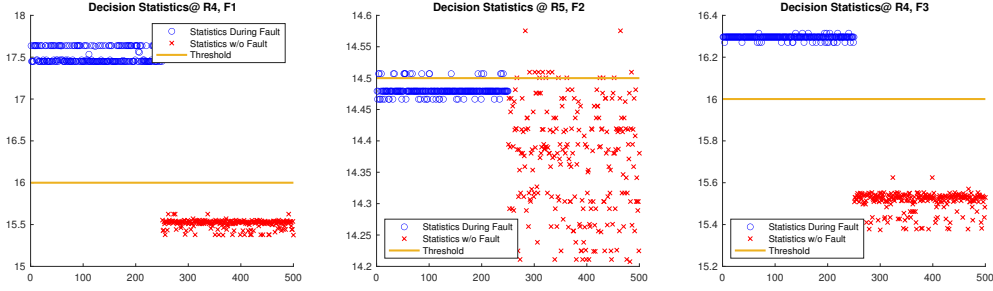


Fig. 9: Scatter Plot of Decision Statistics used in the conventional protection method. In other words, the maximum current magnitude.

The leftmost panel shows the case of F1 at R4, where the current magnitude showed a slight increase due to the presence of SDG. This challenges the detection accuracy of the conventional method, where the decision is made solely based on the current magnitude. As seen from the leftmost panel of Fig. 9, since the magnitude of current during fault at R4 is higher than its no-fault counterpart, R4 trips 100% of the times,

leading to the sympathetic tripping phenomenon. A similar pattern is shown under the case F3 at R4, as supported by the rightmost panel.

The middle panel displays the current magnitude under the case of F2 at R5. Due to R5's geographical closeness to the SDG, the no-fault current at R5 exhibits great randomness, and the fault current is decreased compared to the no-SDG counterpart, as supported by the middle panel of Fig. 9. Hence, achieving high TPRs while maintaining FPRs smaller than 5% is not attainable with a single pre-set threshold.

Test statistics under AOCR: AOCR compares current maximum magnitude with an adaptively chosen threshold. We plotted the difference between the maximum current magnitude and the adaptively chosen thresholds in each decision block in Fig. 9. A difference greater than 0 implies fault for AOCR.

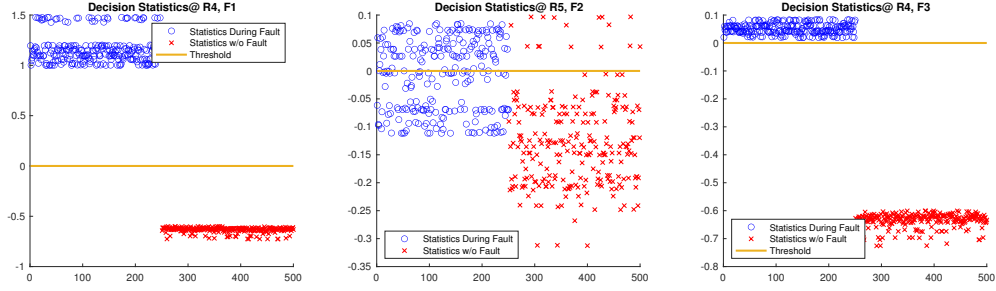


Fig. 10: Scatter Plot of Decision Statistics used in the AOCR.

The decision statistics shown in the leftmost panel of Fig. 10 was obtained under the case F1 at R4, where SDG induced an increase of fault current at R4, who shouldn't trip during fault. Though AOCR computes the decision threshold adaptively, it is still comparing pre-fault and post-fault current magnitudes at R4. The statistics show that the discrepancy between anomaly-free and anomalous cases is smaller using AOCR rather than the conventional method, but the current magnitude increase's negative impact on decision statistics persists. For 100% of its time, the current magnitude at R4 exceeds the adaptive threshold computed based on a 10-second moving average of pre-fault current.

The middle panel displays the current magnitude under the case of F2 at R5, where R5's geographical closeness to the SDG introduces great randomness to the no-fault current. The fault current witnesses a decrease in magnitude compared to the no-SDG counterpart, leading to inaccurate detection results. Though AOCR tries to mitigate the problem by choosing the threshold adaptively, it cannot accommodate high volatility in SGD's output power, thus resulting in lower detection accuracy.

5 Conclusion

The future power grid will be dominated by power electronics-operated energy resources with fast dynamics and rich stochasticity. The state-of-the-art grid monitoring and control is ill-equipped to address formidable challenges brought by large-scale

integration of renewables, multi-sector electrification, and climate-change-induced natural disasters. Therefore, next-generation monitoring must be based on synchronized CPOW measurements to provide high-fidelity and high-resolution situational awareness and control. To this end, this paper offers an approach to compression and interactive networking of CPOW data streaming integrated with data analytics at local IED and control centers.

Acknowledgement

For this special issue in memory of the late Professor Bob Thomas, the first author (Lang Tong) wishes to acknowledge Professor Thomas's contribution to the work presented here over numerous conversations. Professor Thomas was pivotal in the first author's transition to teaching and research in renewable energy, electricity markets, power systems, and smart grid. His presence at Cornell, the Power Systems Engineering Research Center (PSERC), and our research lab is sorely missed.

The authors also wish to acknowledge the contribution of Mei-Jen Lee who performed some of the simulations.

This work was supported in part by the National Science Foundation under Grant EECS-2218110.

References

- [1] Surging Weather-related Power Outages. <https://www.climatecentral.org/climate-matters/surging-weather-related-power-outages>. Accessed:2024-03-08
- [2] A Day Without Power: Outage Costs for Businesses. <https://www.bloomenergy.com/blog/a-day-without-power-outage-costs-for-businesses/>. Accessed: 2024-03-08
- [3] Wiener, N.: Nonlinear Problems in Random Theory. M.I.T. paperback series. MIT Press, Cambridge, MA (1958). <https://books.google.com/books?id=HQBRAAAAMAAJ>
- [4] Masani, P.: Wiener's contributions to generalized harmonic analysis, prediction theory and filter theory. Bulletin of the American Mathematical Society **72**(1.P2), 73–125 (1966)
- [5] Wang, X., Liu, Y., Tong, L.: Adaptive subband compression for streaming of continuous point-on-wave and pmu data. IEEE Transactions on Power Systems **36**(6), 5612–5621 (2021) <https://doi.org/10.1109/TPWRS.2021.3072882>
- [6] Silverstein, A., Follum, J.: High-resolution, time-synchronized grid monitoring devices. Technical Report NASPI-2020-TR-004, North American Synchrophasor Initiative (2020). https://www.naspi.org/sites/default/files/reference-documents/pnnl_29770_naspi_hires_synch_grid_devices_20200320.pdf

- [7] Anderson, P.M., Agrawal, B.L., Van Ness, J.E.: Subsynchronous Resonance in Power Systems. John Wiley & Sons, New York (1999)
- [8] Perez, J.: A guide to digital fault recording event analysis. In: Proc. 63rd Annu. Conf. Protective Relay Engineers, pp. 1–17 (2010)
- [9] Bastos, A.F., Santoso, S., Freitas, W., Xu, W.: Synchrowaveform measurement units and applications. In: 2019 IEEE Power & Energy Society General Meeting (PESGM), Atlanta, GA, USA, pp. 1–5 (2019). <https://doi.org/10.1109/PESGM40551.2019.8973736>
- [10] Carroll, J.R.: A Practical Approach to Streaming Point-on-Wave Data. https://www.naspi.org/sites/default/files/2019-04/04_gpa_carroll_practical_approach_pow_20190417.pdf. Accessed: 2024–03-09 (2019)
- [11] Rahmatian, F.: Point on Wave Measurements, Introduction. https://www.naspi.org/sites/default/files/2019-04/01_nugrid_rahmatian_pow_measurements_intro_20190416.pdf. Accessed: 2024–03-09 (2019)
- [12] Izadi, M., Mohsenian-Rad, H.: Event location identification in distribution networks using waveform measurement units. In: 2020 IEEE PES Innovative Smart Grid Technologies Europe (ISGT-Europe), The Hague, Netherlands, pp. 924–928 (2020). <https://doi.org/10.1109/NAPS58826.2023.10318763>
- [13] Xu, W., Huang, Z., Xie, X., Li, C.: Synchronized waveforms – a frontier of data-based power system and apparatus monitoring, protection, and control. *IEEE Transactions on Power Delivery* **37**(1), 3–17 (2022) <https://doi.org/10.1109/TPWRD.2021.3072889>
- [14] Mohsenian-Rad, H., Xu, W.: Synchro-waveforms: A window to the future of power systems data analytics. *IEEE Power and Energy Magazine* **21**(5), 68–77 (2023)
- [15] Kailath, T.: The Innovations Approach to Detection and Estimation Theory. *Proceedings of the IEEE* **58**(5), 680–695 (1970) <https://doi.org/10.1109/PROC.1970.7723>
- [16] Wang, X., Tong, L.: Innovations Autoencoder and its Application in One-class Anomalous Sequence Detection. arXiv:2106.12382 (2021). <https://arxiv.org/abs/2106.12382>
- [17] Sheskin, D.J.: Handbook of Parametric and Nonparametric Statistical Procedures, Fifth Editio (5th Ed.). Chapman and Hall/CRC, Boca Raton (2011). <https://doi.org/10.1201/9780429186196>
- [18] Sheskin, D.J.: Handbook of Parametric and Nonparametric Statistical Procedures, 4th edn. Chapman & Hall/CRC, ??? (2007)

- [19] Ma, J., Perkins, S.: Time-series Novelty Detection Using One-class Support Vector Machines. In: Proceedings of the International Joint Conference on Neural Networks, 2003., vol. 3, pp. 1741–17453 (2003). <https://doi.org/10.1109/IJCNN.2003.1223670>
- [20] Dasgupta, D., Forrest, S.: Novelty Detection in Time Series Data using Ideas from Immunology. In: In Proceedings of The International Conference on Intelligent Systems (1995)
- [21] Gardner, A.B., Krieger, A.M., Vachtsevanos, G., Litt, B.: One-Class Novelty Detection for Seizure Analysis from Intracranial EEG. *Journal of Machine Learning Research* **7**(37), 1025–1044 (2006)
- [22] Schölkopf, B., Williamson, R., Smola, A., Shawe-Taylor, J., Platt, J.: Support Vector Method for Novelty Detection. *Proceedings of the 12th International Conference on Neural Information Processing Systems*, 582–588 (1999)
- [23] Khan, S.S., Madden, M.G.: One-class Classification: Taxonomy of Study and Review of Techniques. *The Knowledge Engineering Review* **29**(3), 345–374 (2014) <https://doi.org/10.1017/S026988891300043X>
- [24] Bergmann, P., Löwe, S., Fauser, M., Sattlegger, D., Steger, C.: Improving Unsupervised Defect Segmentation by Applying Structural Similarity to Autoencoders. *Proceedings of the 14th International Joint Conference on Computer Vision, Imaging and Computer Graphics Theory and Applications* (2019) <https://doi.org/10.5220/0007364503720380>
- [25] Gong, D., Liu, L., Le, V., Saha, B., Mansour, M.R., Venkatesh, S., Hengel, A.: Memorizing Normality to Detect Anomaly: Memory-augmented Deep Autoencoder for Unsupervised Anomaly Detection (2019)
- [26] Lee, K., Lee, H., Lee, K., Shin, J.: Training Confidence-calibrated Classifiers for Detecting Out-of-Distribution Samples. In: *International Conference on Learning Representations* (2018). <https://openreview.net/forum?id=ryiAv2xAZ>
- [27] Hendrycks, D., Mazeika, M., Dietterich, T.: Deep Anomaly Detection with Outlier Exposure. In: *International Conference on Learning Representations* (2019). <https://openreview.net/forum?id=HyxCxhRcY7>
- [28] Ren, J., Liu, P.J., Fertig, E., Snoek, J., Poplin, R., DePristo, M.A., Dillon, J.V., Lakshminarayanan, B.: Likelihood Ratios for Out-of-Distribution Detection. *arXiv:1906.02845* (2019). <https://arxiv.org/abs/1906.02845>
- [29] Hendrycks, D., Gimpel, K.: A baseline for detecting misclassified and out-of-distribution examples in neural networks. In: *International Conference on Learning Representations* (2017). <https://openreview.net/forum?id=Hkg4TI9xl>

- [30] Lakshminarayanan, B., Pritzel, A., Blundell, C.: Simple and scalable predictive uncertainty estimation using deep ensembles. In: Guyon, I., Luxburg, U.V., Bengio, S., Wallach, H., Fergus, R., Vishwanathan, S., Garnett, R. (eds.) *Advances in Neural Information Processing Systems*, vol. 30. Curran Associates, Inc., ??? (2017). https://proceedings.neurips.cc/paper_files/paper/2017/file/9ef2ed4b7fd2c810847ffa5fa85bce38-Paper.pdf
- [31] Liang, S., Li, Y., Srikant, R.: Enhancing the Reliability of Out-of-distribution Image Detection in Neural Networks. (2018). Funding Information: The research reported here was supported by NSF Grant CPS ECCS 1739189. Publisher Copyright: © Learning Representations, ICLR 2018 - Conference Track Proceedings. All right reserved.; 6th International Conference on Learning Representations, ICLR 2018 ; Conference date: 30-04-2018 Through 03-05-2018
- [32] Lee, K., Lee, K., Lee, H., Shin, J.: A Simple Unified Framework for Detecting Out-of-Distribution Samples and Adversarial Attacks. In: Bengio, S., Wallach, H., Larochelle, H., Grauman, K., Cesa-Bianchi, N., Garnett, R. (eds.) *Advances in Neural Information Processing Systems*, vol. 31. Curran Associates, Inc., ??? (2018). <https://proceedings.neurips.cc/paper/2018/file/abdeb6f575ac5c6676b747bca8d09cc2-Paper.pdf>
- [33] Le Lan, C., Dinh, L.: Perfect density models cannot guarantee anomaly detection. *Entropy* **23**(12) (2021) <https://doi.org/10.3390/e23121690>
- [34] Schlegl, T., Seeböck, P., Waldstein, S.M., Langs, G., Schmidt-Erfurth, U.: f-anogan: Fast unsupervised anomaly detection with generative adversarial networks. *Medical Image Analysis* **54**, 30–44 (2019) <https://doi.org/10.1016/j.media.2019.01.010>
- [35] Dinh, L., Krueger, D., Bengio, Y.: NICE: Non-linear Independent Components Estimation. *arXiv:arXiv:1410.8516* (2015). <https://arxiv.org/abs/1410.8516>
- [36] Brakel, P., Bengio, Y.: Learning Independent Features with Adversarial Nets for Non-linear ICA. *arXiv:1710.05050* (2017)
- [37] Sricharan, K., Hero, A.: Efficient anomaly detection using bipartite k-nn graphs. In: Shawe-Taylor, J., Zemel, R., Bartlett, P., Pereira, F., Weinberger, K.Q. (eds.) *Advances in Neural Information Processing Systems*, vol. 24. Curran Associates, Inc., ??? (2011). https://proceedings.neurips.cc/paper_files/paper/2011/file/8dd48d6a2e2cad213179a3992c0be53c-Paper.pdf
- [38] Chen, H.: Sequential change-point detection based on nearest neighbors. *The Annals of Statistics* **47**(3), 1381–1407 (2019) <https://doi.org/10.1214/18-AOS1718>
- [39] Chen, H., Chu, L.: Graph-based change-point analysis. *Annual Review of Statistics and Its Application* **10**(1), 475–499 (2023) <https://doi.org/10.1214/18-AOS1718>

[org/10.1146/annurev-statistics-122121-033817](https://doi.org/10.1146/annurev-statistics-122121-033817) <https://doi.org/10.1146/annurev-statistics-122121-033817>

- [40] Zhou, H., Zhang, S., Peng, J., Zhang, S., Li, J., Xiong, H., Zhang, W.: Informer: Beyond efficient transformer for long sequence time-series forecasting. *Proceedings of the AAAI Conference on Artificial Intelligence* **35**(12), 11106–11115 (2021) <https://doi.org/10.1609/aaai.v35i12.17325>
- [41] Zeng, A., Chen, M., Zhang, L., Xu, Q.: Are transformers effective for time series forecasting? In: *Proceedings of the Thirty-Seventh AAAI Conference on Artificial Intelligence and Thirty-Fifth Conference on Innovative Applications of Artificial Intelligence and Thirteenth Symposium on Educational Advances in Artificial Intelligence. AAAI’23/IAAI’23/EAAI’23*. AAAI Press, ??? (2023). <https://doi.org/10.1609/aaai.v37i9.26317> . <https://doi.org/10.1609/aaai.v37i9.26317>
- [42] Wang, X., Tong, L., Zhao, Q.: Generative Probabilistic Price Forecasting via Weak Innovations. Submitted for publications. See updated preprint at [arXiv](https://arxiv.org/abs/2024.01.18) (2024)
- [43] Mestav, K.R., Wang, X., Tong, L.: A deep learning approach to anomaly sequence detection for high-resolution monitoring of power systems. *IEEE Transactions on Power Systems* **38**(1), 4–13 (2023) <https://doi.org/10.1109/TPWRS.2022.3168529>
- [44] D’Agostino, R.B.: *Goodness-of-Fit-Techniques*. (First Edition). Taylor and Francis, London (2017). <https://www.taylorfrancis.com/books/9780203753064>
- [45] Neyman, J.: "smooth test" for goodness of fit. *Scandinavian Actuarial Journal* **1937**(3-4), 149–199 (1937) <https://doi.org/10.1080/03461238.1937.10404821> <https://doi.org/10.1080/03461238.1937.10404821>
- [46] Rayner, J.C.W., Best, D.J.: Smooth tests of goodness of fit: An overview. *International Statistical Review / Revue Internationale de Statistique* **58**(1), 9–17 (1990). Accessed 2024-01-18
- [47] Cover, T.M., Thomas, J.A.: *Elements of Information Theory*. (2nd Ed.). Wiley-Interscience, Hoboken, New Jersey (2006). <https://resolver.ebscohost.com/Redirect/PRL?EPPackageLocationID=2106155.274641.21607325&epcustomerid=s9001366>
- [48] Gersho, A., Gray, R.M.: *Vector Quantization and Signal Compression*. Kluwer Academic Publishers, Boston (1992). <https://resolver.ebscohost.com/Redirect/PRL?EPPackageLocationID=7191.30710607.5628611&epcustomerid=s9001366>
- [49] Telukunta, V., Pradhan, J., Agrawal, A., Singh, M., Srivani, S.G.: Protection Challenges under Bulk Penetration of Renewable Energy Resources in Power Systems: A Review. *CSEE Journal of Power and Energy Systems* **3**(4), 365–379 (2017) <https://doi.org/10.17775/CSEEJPES.2017.00030>

- [50] Anderson, P.M.: Power System Protection. McGraw-Hill, New York (1999)
- [51] El-Khattam, W., Sidhu, T.S.: Restoration of Directional Overcurrent Relay Coordination in Distributed Generation Systems Utilizing Fault Current Limiter. *IEEE Transactions on Power Delivery* **23**(2), 576–585 (2008) <https://doi.org/10.1109/TPWRD.2008.915778>
- [52] Ibrahim, D.K., Zahab, E., Mostafa, S.: New Coordination Approach to Minimize the Number of Re-adjusted Relays when Adding DGs in Interconnected Power Systems with a Minimum Value of Fault Current Limiter. *International Journal of Electrical Power & Energy Systems* **85**, 32–41 (2017) <https://doi.org/10.1016/j.ijepes.2016.08.003>
- [53] Chattopadhyay, B., Sachdev, M.S., Sidhu, T.S.: An On-line Relay Coordination Algorithm for Adaptive Protection using Linear Programming Technique. *IEEE Transactions on Power Delivery* **11**(1), 165–173 (1996) <https://doi.org/10.1109/61.484013>
- [54] Liu, Z., Hoidalén, H.K., Saha, M.M.: An Intelligent Coordinated Protection and Control Strategy for Distribution Network with Wind Generation Integration. *CSEE Journal of Power and Energy Systems* **2**(4), 23–30 (2016) <https://doi.org/10.17775/CSEEJPES.2016.00045>
- [55] Wan, H., Li, K.K., Wong, K.P.: An Adaptive Multiagent Approach to Protection Relay Coordination With Distributed Generators in Industrial Power Distribution System. *IEEE Transactions on Industry Applications* **46**(5), 2118–2124 (2010) <https://doi.org/10.1109/TIA.2010.2059492>
- [56] Papaspiliotopoulos, V.A., Korres, G.N., Kleftakis, V.A., Hatziaargyriou, N.D.: Hardware-In-the-Loop Design and Optimal Setting of Adaptive Protection Schemes for Distribution Systems With Distributed Generation. *IEEE Transactions on Power Delivery* **32**(1), 393–400 (2017) <https://doi.org/10.1109/TPWRD.2015.2509784>
- [57] Rezaei, S.: Intelligent Overcurrent Protection During Ferroresonance in Smart Distribution Grid. In: 2019 IEEE International Conference on Environment and Electrical Engineering and 2019 IEEE Industrial and Commercial Power Systems Europe (EEEIC / I CPS Europe), pp. 1–6 (2019). <https://doi.org/10.1109/EEEIC.2019.8783752>
- [58] Shen, S., Lin, D., Wang, H., Hu, P., Jiang, K., Lin, D., He, B.: An Adaptive Protection Scheme for Distribution Systems With DGs Based on Optimized Thevenin Equivalent Parameters Estimation. *IEEE Transactions on Power Delivery* **32**(1), 411–419 (2017) <https://doi.org/10.1109/TPWRD.2015.2506155>
- [59] Ma, J., Wang, X., Zhang, Y., Yang, Q., Phadke, A.G.: A Novel Adaptive Current

Protection Scheme for Distribution Systems with Distributed Generation. *International Journal of Electrical Power & Energy Systems* **43**(1), 1460–1466 (2012) <https://doi.org/10.1016/j.ijepes.2012.07.024>

- [60] Liu, Z., Su, C., Høidalen, H.K., Chen, Z.: A Multiagent System-Based Protection and Control Scheme for Distribution System With Distributed-Generation Integration. *IEEE Transactions on Power Delivery* **32**(1), 536–545 (2017) <https://doi.org/10.1109/TPWRD.2016.2585579>
- [61] Mahat, P., Chen, Z., Bak-Jensen, B., Bak, C.L.: A Simple Adaptive Overcurrent Protection of Distribution Systems With Distributed Generation. *IEEE Transactions on Smart Grid* **2**(3), 428–437 (2011) <https://doi.org/10.1109/TSG.2011.2149550>
- [62] Fawzi, O., Flammarion, N., Garivier, A., Oufkir, A.: Sequential algorithms for testing identity and closeness of distributions (2022)
- [63] Ieee standard for inverse-time characteristics equations for overcurrent relays. *IEEE Std C37.112-2018* (Revision of IEEE Std C37.112-1996), 1–25 (2019) <https://doi.org/10.1109/IEEESTD.2019.8635630>
- [64] Jain, R., Lubkeman, D.L., Lukic, S.M.: Dynamic adaptive protection for distribution systems in grid-connected and islanded modes. *IEEE Transactions on Power Delivery* **34**(1), 281–289 (2019) <https://doi.org/10.1109/TPWRD.2018.2884705>